# Measurement of a rotary mechanical pulsation compensator under hydraulic resonance

David Holzer and Gudrun Mikota

Institute of Machine Design and Fluid Power, Johannes Kepler University, Linz, Austria
E-mail: david.holzer@jku.at, gudrun.mikota@jku.at

## Abstract

If the pulsation frequency of a hydraulic pump or motor coincides with a natural frequency of the hydraulic system, there is a particular need for pulsation compensation. Under these conditions, a rotary mechanical pulsation compensator is investigated. The compensator consists in a torsional oscillator which is formed by the drivetrain of a radial piston pump and requires a special compensator coupling. At the pump outlet, two different hydraulic layouts are considered, including a closed pipeline and a cylinder chamber connected via a hose. Prior to experiments, simulations are conducted to determine system parameters at which a natural frequency of the hydraulic system matches the compensation frequency. In the experimental setup, the compensator coupling is installed on the pump shaft and driven by a speed-controlled induction motor. The measurements conducted with a closed pipeline show a pulsation reduction by a factor of more than three in the resonance case during a run-up test. Similar results are obtained in a run-up test with a cylinder in its limit stop position. An extension test with constant motor speed shows significant reduction of pressure pulsation. In the present configuration, the compensation effect is narrowband and the design of the coupling causes a dependency between compensation frequency and drivetrain torque.

**Keywords:** pulsation, radial piston pump, drivetrain, compensator, coupling, resonance

## 1 Introduction

The noise generated by hydraulic systems, both in industrial applications and in mobile machinery, represents a significant disadvantage. Noise is caused by pressure pulsations in the fluid, which lead to mechanical vibrations. As explained in [1], pressure pulsations arise both from the operating principles of positive displacement machines and from external vibrations acting on hydraulic components. If the pulsation frequency of a pump or motor matches a natural frequency of the system, resonance will occur, which amplifies the pressure pulsation and increases the noise. Under such resonance conditions, the need for countermeasures is most apparent.
To reduce hydraulic pressure pulsation, there are both active and passive concepts. Passive attenuators are significantly more widespread than active solutions and operate based on resistive, reactive or composite working principles. Resistive damping attenuators work over an unlimited frequency range but cause high energy losses in the system. In contrast, reactive compensators have a limited frequency range [2]. These compensators are designed as oscillating systems, with the compensator system's natural frequency tuned to the disturbing pulsation frequency. At this frequency, the compensator oscillates in anti-phase with the pump or motor pulsation. A well-known example of this type of compensator is the Helmholtz resonator. It is based on a hydraulic oscillator consisting of an inductance and a capacity. The passive compensator described in [3] replaces the hydraulic resonator with a mechanical spring-mass oscillator placed in the hydraulic circuit.
The present paper investigates a special coupling installed on the pump shaft, which turns the pump drivetrain into a rotary mechanical pulsation compensator [4] modelled by a two-mass torsional oscillator. This oscillator consists of the mass moment of inertia on the drive side, the mass moment of inertia on the pump side and the stiffness of the designed compensator coupling. Starting from the simulations and design from [5, 6], the compensator coupling was designed for an existing experimental setup. It was fabricated and installed in the test rig. Initial measurements were carried out, which already showed a compensation effect [7].
In order to study the properties of the compensator coupling in the case of hydraulic resonance, measurements were conducted on two different hydraulic layouts and are presented in this paper.

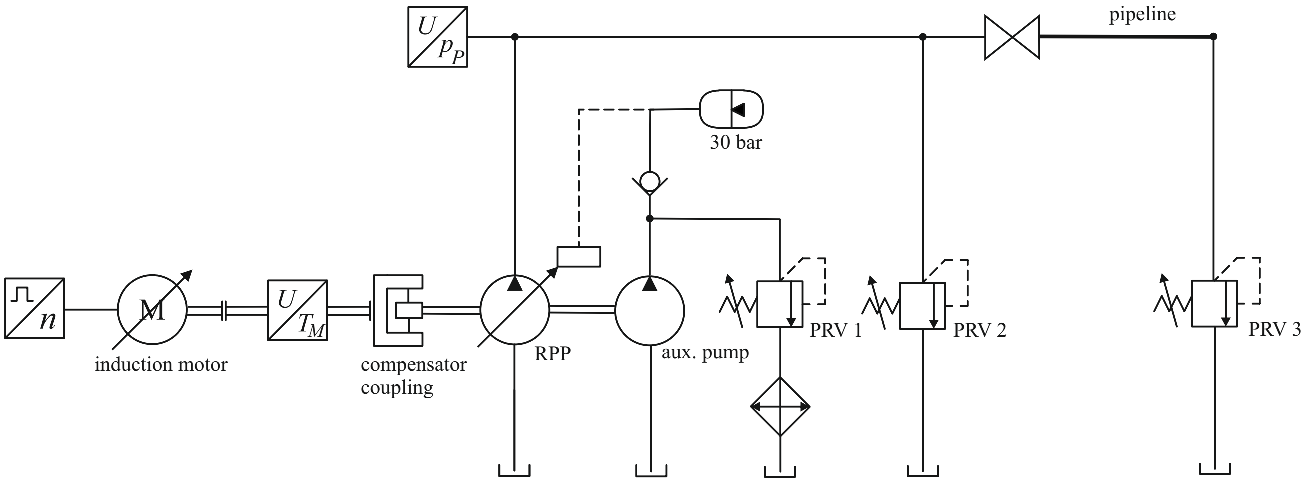


*Figure 1: Overall hydraulic layout including the drivetrain, with compensator coupling and a closed pipeline.*

## 2 Experimental test setup

The experimental setup is driven by a speed-controlled induction motor with a rated speed of 1420 rpm and a rated torque of 71.3 Nm. To measure the drivetrain torque, a measuring shaft is installed after the motor. The connections between the motor, the measuring shaft and the compensator coupling are realised by curved tooth couplings. The compensator coupling is installed directly on the pump shaft via a key connection. The structure of the drivetrain is shown in fig. 1 as simplified hydraulic circuit diagram and in fig. 2 as photo.

The radial piston pump used in this test rig is shown in fig. 3. It has seven pistons and variable displacement with a maximum of 32 $cm^3$ / rev. To adjust the displacement via the stroke ring, an auxiliary gear pump is required as pressure supply. The stroke ring, which is controlled by a servo valve, is set to maximum displacement for all experiments. It is necessary to keep the oil temperature within a narrow range for the tests, as preliminary tests have shown that the dependence between oil temperature and pressure pulsation cannot be neglected. Pressure pulsation increases with higher oil temperatures. Most of the heat is generated by the pressure relief valve in the main circuit (PRV 2 in fig. 1), depending on the set pressure. To effectively cool the system between tests without adjusting the setting of the pressure relief valve PRV2, the cooling system is installed in the return line of the auxiliary pump. The circuit of the auxiliary pump can be operated separately by adjusting the radial piston pump to zero displacement. The pressure of the auxiliary pump is limited by a pressure relief valve (PRV 1 in fig. 1) to around 30 bar, which is near the minimal pressure for the stroke ring adjustment. Actually, the auxiliary circuit is designed for higher pressures, but the lower pressure helps to prevent excessive heating of the oil and reduces the required motor torque.

The pressure in the main hydraulic circuit is limited by the pressure relief valve PRV2 (installed at the outlet of the radial piston pump). To protect the compensator coupling prototype and to prevent overloading the electric motor, the maximum permissible pressure in the main hydraulic circuit is limited to 130 bar.

To investigate the compensator coupling under hydraulic resonance conditions, two different hydraulic systems installed downstream of the shut-off valve are considered. The first one includes a closed pipeline and is shown in fig. 1. The explanation of this hydraulic system is provided in Section 4.1. The second one includes a hydraulic cylinder (see fig. 14).

For measurement data acquisition, the test rig is equipped with an incremental encoder to record the angular motor position, a torque measurement shaft, and a pressure sensor at the pump outlet. All measurements are conducted with a sampling rate of 5 kHz.

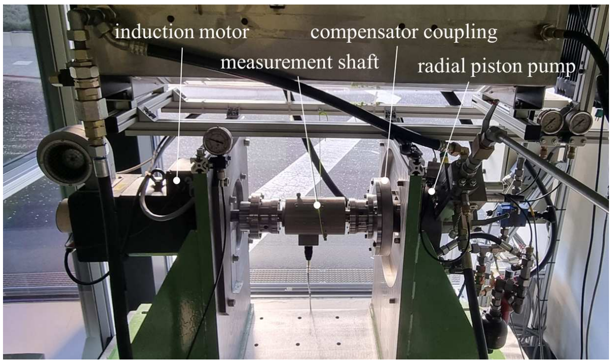


*Figure 2: Test rig with compensator coupling.*

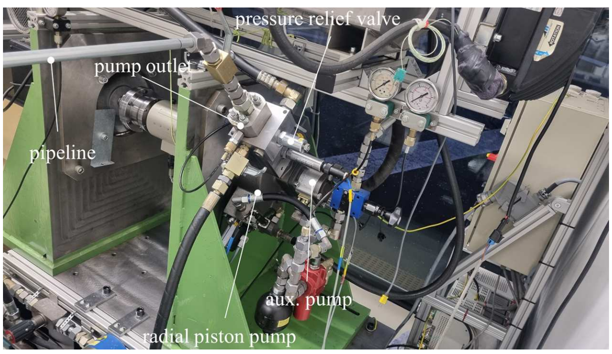


*Figure 3: Radial piston pump and outlet block.*

*Figure 4: Compensator coupling.*

## 3 Compensator coupling

The compensator coupling prototype consists of a spoke wheel and a flange. The assembled compensator coupling is shown in fig. 4. Inner and outer ring of the spoke wheel are connected through radial beams. For calculating the compensation frequency, the drivetrain is modelled as two-mass torsional oscillator. The mass moment of inertia $I_M$ of the motor side contains the inertia of the motor, the measuring shaft including the curved tooth couplings, the flange and the outer ring. The mass moment of inertia $I_P$ on the pump side includes the inertia of the inner ring, the radial piston pump and the auxiliary pump. With a compensation frequency $f_C$, the required stiffness of the compensator coupling is given by

$$k_T = (2\pi f_C)^2 \frac{I_M I_P}{I_M + I_P}. \tag{1}$$

For the initial design of the compensator, the radial beams were treated as bending beams according to first-order theory. This calculation was performed in [6]. As a result of this consideration, the stiffness of the compensator coupling would only depend on material parameters and dimensions. To understand the actual behaviour of the coupling, measurements have been carried out at eight different system pressures, corresponding to eight different torque values in the drivetrain. The pressure levels were set by adjusting the pressure relief valve PRV2 according to fig. 1. To excite the frequency range under investigation, the motor speed was increased linearly from 850 rpm to 1700 rpm. For the determination of the compensation frequency $f_C$, the signal of the pump pressure $p_P$ was transferred into the frequency domain using Fourier Transformation. More details of the test procedure are described in section 4. Figure 5 demonstrates the determination of compensation frequencies through four selected measurement results of the pump pressure $p_P$ in the frequency domain. In each signal at least two local minima of the amplitude occur. In each measurement a reduction of the amplitude occurs in the frequency range around 162 Hz, which is not caused by the compensator. This is discussed in more detail in section 4.1. The lower anti-resonance frequency varies between the different experiments. The red line in fig. 5 illustrates the result of experiment 1 from tab. 1, with the compensation frequency of 137.2 Hz at a pump pressure of 60.6 bar. In contrast the purple line shows the result of experiment 8, with a pump pressure of 122.2 bar and a detected compensation frequency of 153.6 Hz.

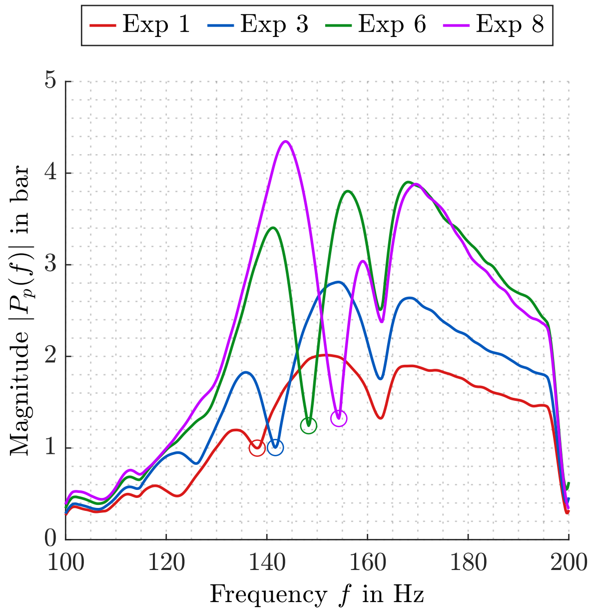


*Figure 5: Frequency Spectra of selected measurement results.*

The results for all eight different system pressures are summarized in tab. 1, which includes the torque $T_M$ in the drivetrain and the compensation frequency $f_C$ at the pump pressure $p_P$. It is evident that the compensation frequency increases with increasing torque. This suggests that the modelling with first-order theory is only a rough approximation for the calculation of a compensator coupling, as it cannot account for the dependency on the torque. Second-order theory would include normal stresses that increase stiffness with increasing angular displacement, leading to torque dependence. In the investigated pump pressure range from approximately 60 bar to 120 bar, the compensation frequency increases by 12.7 %.

*Table 1: Dependence of the compensation frequency.*

| Number | Pump pressure $p_P$ | Drivetrain torque $T_M$ | Compensation frequency $f_C$ |
|---|---|---|---|
| Exp 1 | 60.6 bar | 41.4 Nm | 138.1 Hz |
| Exp 2 | 71.8 bar | 46.8 Nm | 139.9 Hz |
| Exp 3 | 83.7 bar | 53.0 Nm | 141.7 Hz |
| Exp 4 | 94.5 bar | 57.3 Nm | 144.7 Hz |
| Exp 5 | 100.6 bar | 61.4 Nm | 146.7 Hz |
| Exp 6 | 105.8 bar | 65.1 Nm | 148.3 Hz |
| Exp 7 | 117.9 bar | 71.2 Nm | 151.9 Hz |
| Exp 8 | 122.2 bar | 74.3 Nm | 154.3 Hz |

As opposed to the motor, the mass geometry of the pump is not known. To verify the dynamic measurements and estimate the mass moment of inertia of the pump side, static tests and finite element (FEM) analyses were conducted to determine the stiffness $k_T$. The results are shown in tab. 2. The stiffness values from measurements and FEM analyses match well. Therefore, the mass moment of inertia of the pump side is approximated for the torques given in tab. 1, using the stiffness calculated from FEM analyses and the measured frequencies. The resulting value is approximately $3.1 \cdot 10^{-3}$ kg m$^2$.

*Table 2: Identification of stiffness $k_T$.*

| Static torque | Measured stiffness | FEM stiffness |
|---|---|---|
| 50 Nm | 2540 Nm/rad | 2470 Nm/rad |
| 75 Nm | 2990 Nm/rad | 2920 Nm/rad |

## 4 Hydraulic system with closed pipeline

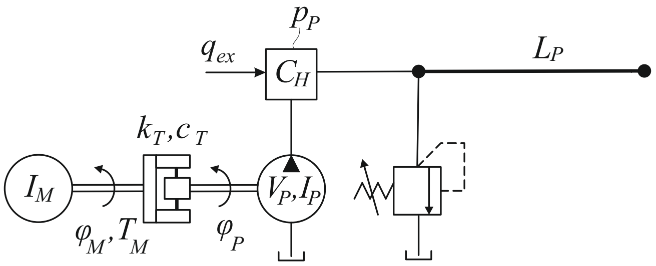


*Figure 6: Hydraulic system with pipeline.*

To design an experimental setup with a resonance frequency near the compensation frequency, the system is initially simulated in the frequency domain. Figure 6 shows a schematic of the hydraulic system with a closed pipeline including all components considered in the model. The pressure relief valves and the auxiliary pump are neglected. The system contains a closed hydraulic pipeline with a length $L_p$ on the pump outlet. The coupled hydraulic-mechanical model, which is described more closely in [5], can be written as

$$\left(-\omega^2 \mathbf{M} + i\omega \mathbf{C} + \mathbf{K}\right) \mathbf{X}(i\omega) = \mathbf{F}(i\omega) \tag{2}$$

with the mass matrix $\mathbf{M}$, the damping matrix $\mathbf{C}$, the stiffness matrix $\mathbf{K}$, the state vector $\mathbf{X}$ and the excitation vector $\mathbf{F}$. In explicit form they read

$$\mathbf{M} = \begin{bmatrix} I_M & 0 & 0 \\ 0 & I_P & 0 \\ 0 & -\frac{V_p}{2\pi} & C_H \end{bmatrix}, \quad \mathbf{C} = \begin{bmatrix} 0 & 0 & 0 \\ 0 & c_T & 0 \\ 0 & 0 & S_{12} \end{bmatrix},$$

$$\mathbf{K} = \begin{bmatrix} k_T & -k_T & 0 \\ -k_T & k_T & \frac{V_P}{2\pi} \\ 0 & 0 & 0 \end{bmatrix}, \tag{3}$$

$$\mathbf{X} = \begin{bmatrix} \Phi_M(i\omega) \\ \Phi_P(i\omega) \\ P_P(i\omega) \end{bmatrix}, \quad \mathbf{F} = \begin{bmatrix} T_M(i\omega) \\ 0 \\ i\omega Q_{ex}(i\omega) \end{bmatrix}.$$

The states of the linear model are the rotation angle of the motor $\Phi_M$, the rotation angle of the pump $\Phi_P$ and the pressure at pump outlet $P_P$. $T_M$ describes the moment of the electric motor and $Q_{ex}$ represents the flow rate pulsation caused by the pump mechanism. $V_P$ describes the displacement of the radial piston pump, $C_H$ the hydraulic capacity of the pump outlet block and $c_T$ the torsional damping of the compensator coupling. The function

$$S_{12} = \frac{\sinh(\gamma L_P)}{Z \cosh(\gamma L_P)} \tag{4}$$

with

$$Z = \frac{\sqrt{E\rho}}{r_P^2 \pi} \sqrt{-\frac{J_0(ir\sqrt{i\omega/\nu})}{J_2(ir\sqrt{i\omega/\nu})}} \tag{5}$$

and

$$\gamma = \frac{i\omega}{\sqrt{E/\rho}} \sqrt{-\frac{J_0(ir\sqrt{i\omega/\nu})}{J_2(ir\sqrt{i\omega/\nu})}} \tag{6}$$

considers the closed-end pipeline by a dynamic laminar pipeline model as developed in [8]. $J_0$ and $J_2$ are Bessel functions of first kind. The parameters for the simulation are given in tab. 3. To account for additional damping in the hydraulic system e.g. at bends or junctions, the kinematic viscosity is increased from 32 m$^2$ s$^{-1}$ to 100 m$^2$ s$^{-1}$ for the simulations. The damping of the pump rotor $c_T$ has been estimated in [5]. Only the gap at inner rotor radius is modelled. $c_T$ is increased to account for further sources of damping, e.g. piston $\leftrightarrow$ barrel, slippers or rotor faces $\leftrightarrow$ housing. To ensure that the compensation frequency $f_C$ exactly matches the resonance frequency, the stiffness $k_T$ was calculated using equation (1).

*Table 3: Parameters for the experiment with closed pipeline.*

| | | |
|---|---|---|
| $I_M$ | $158.4 \cdot 10^{-3}$ kg m$^2$ | Inertia motor side |
| $I_P$ | $3.1 \cdot 10^{-3}$ kg m$^2$ | Inertia pump side |
| $V_P$ | 32 cm$^3$ / rev | Displacement volume |
| $V_H$ | 160 cm$^3$ | Volume pump outlet block |
| $E$ | $1.5 \cdot 10^9$ Pa | Bulk modulus |
| $\rho$ | 835 kg m$^{-3}$ | Density |
| $\nu$ | 100 m$^2$ s$^{-1}$ | Kinematic viscosity |
| $c_T$ | 0.5 Nm/rad s | Torsional damping |
| $k_T$ | 2810 Nm/rad | Torsional stiffness |
| $L_P$ | 3.2 m | Pipeline length |
| $r_P$ | 6 mm | Pipeline inner radius |
| $C_H$ | $V_H/E$ | Capacity pump outlet |

The simulation results, as transfer functions between flow rate excitation and pressure response $G_{PQ}(i\omega) = P_P(i\omega)/Q_{ex}(i\omega)$, are shown in fig. 7. The blue line represents the transmission behaviour without compensator coupling. The pipeline length was chosen such that the hydraulic resonance occurs around 150 Hz. In fig. 7, the frequency response with compensator coupling is shown in red. The simulation predicts a clear reduction in magnitude at the compensation frequency. Below and above this frequency, two secondary resonances arise, where the peaks depend on damping. These simulation results suggest that a well-tuned compensator can significantly improve the system behaviour in the resonance case.

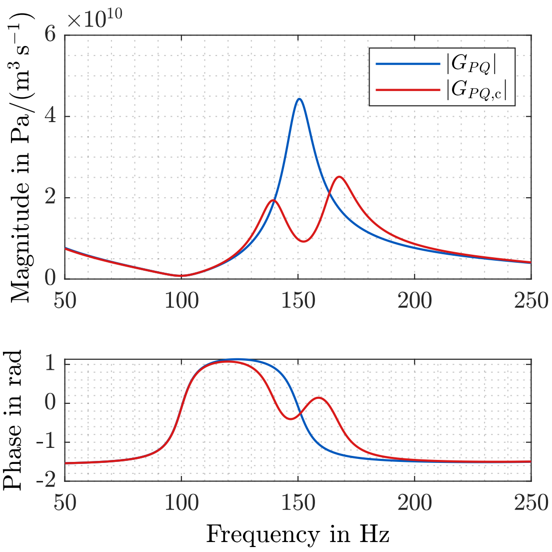


*Figure 7: Simulation results with pipeline as transfer function between flow rate excitation and pressure response. Blue: Without compensator, Red: With compensator.*

### 4.1 Run-up experiment with closed pipeline

Based on the simulation results and the investigation concerning the compensation frequency, the hydraulic system in fig. 1 was tuned for the existing compensator. For this purpose, a 3.25 m long pipeline, including all fittings, was used. The pipeline is shown in fig. 8. To maximize the visibility of the compensator effect, high pulsations are required in hydraulic resonance. A lower oil viscosity reduces the damping of the hydraulic system. Therefore, the oil in the system is heated

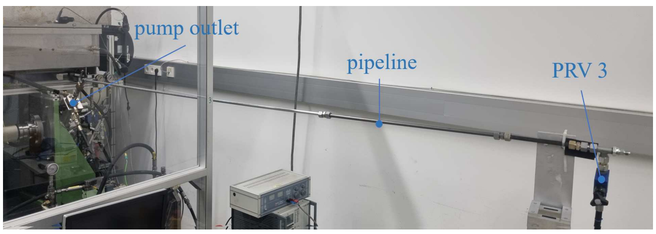


*Figure 8: Hydraulic system with closed pipeline.*

up to approximately 50 °C. To get a uniform oil temperature in both the pipeline and the tank, oil must flow through the pipeline. To achieve this, a pressure relief valve (PRV 3 in fig. 1) is mounted at the end of the pipeline, which is inactive during the measurements. Additionally, it is essential for venting the pipeline.

To analysis the effect of the compensator coupling, the pressure at the pump outlet is evaluated. For a run-up experiment, fig. 9 shows the pump pressure $p_P$ in the time domain. At the top, the signal of the pressure sensor is displayed, in blue without compensator and in red with compensator. To suppress the influence of noise, a low-pass filter with a cut-off frequency of 1000 Hz was used. For better visibility, the envelope of the reference measurement is shown. In the reference measurement the pressure level was around 1.5 bar lower. Due to the flow rate dependence of the pressure relief valve, the pump pressure increases with higher rotational speed. The diagram in the middle of fig. 9 shows the pressure signal filtered with a bandpass filter with a passband frequency from 50 Hz to 250 Hz. In the measurement without the compensator, a significant reduction of the pressure amplitude is observed after 3.5 seconds. At this point, the reference measurement indicates a pressure pulsation amplitude of approximately 4.2 bar. In contrast, the amplitude of the measurement with the compensator is 1.3 bar. This corresponds to an amplitude reduction by a factor of more than three in the resonance case. For the experiment, the rotational speed of the motor was increased with constant acceleration from 850 rpm up to 1700 rpm, as shown at the bottom in fig. 9. At the resonance case, after 3.5 seconds the motor operates at a speed of 1270 rpm. The frequency of the dynamic flow rate pulsation can be calculated as follows:

$$f_{ex} = \frac{n_{mot}}{60} m_p = 148.2\text{Hz}, \tag{7}$$

with the number of pistons $m_p = 7$ and the motor speed $n_{mot}$ in rpm.

For the analysis in the frequency domain, the pump pressure at the pump outlet is transformed using the Short-Time Fourier Transformation (STFT). Figure 10 shows the result of the reference measurement on the top and of the measurement with compensator at the bottom visualised as 3D waterfall plot. The STFT is applied to analyse how the frequency components of the pressure signal evolve during the measurement, as the excitation frequency changes over time. Therefore, the signal is divided into small overlapping time segments, with each segment transformed into the frequency domain using a Fast Fourier Transform (FFT). At the start, an excitation at 100 Hz is observed, and by the end of the measurement, it has shifted to 200 Hz. This corresponds to the motor speed. Higher-order excitations are also visible. The effect of the compensator is clearly noticeable after 3.5 seconds and at a frequency of around 150 Hz.

To simplify the analysis, only the frequency axis is examined. Figure 11 shows the individual Fourier-transformed signals overlaid, with only the maximum values considered. In contrast to fig. 10, the overlap in the STFT was increased to improve the time resolution and obtain a smoother signal. Furthermore, the data points were interpolated cubically. The maximum compensation effect occurs at 148.3 Hz. The calculated excitation frequency matches the measured compensation frequency. This confirms that the dynamic flow rate pulsation excites the system. As described in [9], the geometric flow rate pulsation would have twice this frequency due to the odd number of pistons. In the frequency range between 140 Hz and 155 Hz, the compensator improves the system behaviour. Compared to the simulation results shown in fig. 7, the frequency range in which the compensator coupling improves the system is more narrowband. When comparing measurement and simulation, it must be considered that the simulation represents a transfer function, while the measurement reflects a system response. In the simulation, a constant excitation

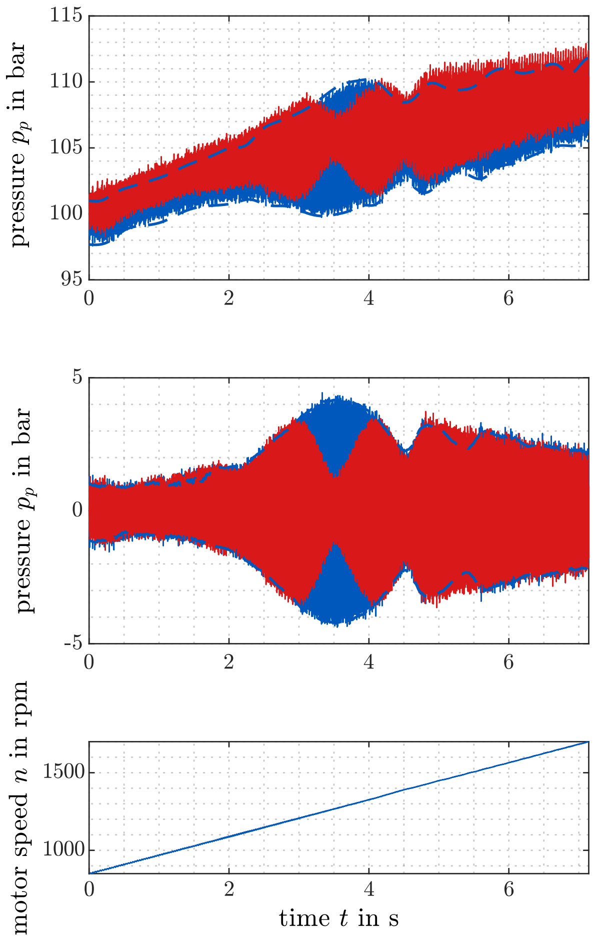


*Figure 9: Measurement results of the run-up experiment with closed pipeline, Blue: Without compensator, Red: With compensator, Top: Low-pass filtered signal of the pressure on the pump outlet, Middle: Bandpass filtered pressure signal at the pump outlet, Bottom: Motor rotation speed.*

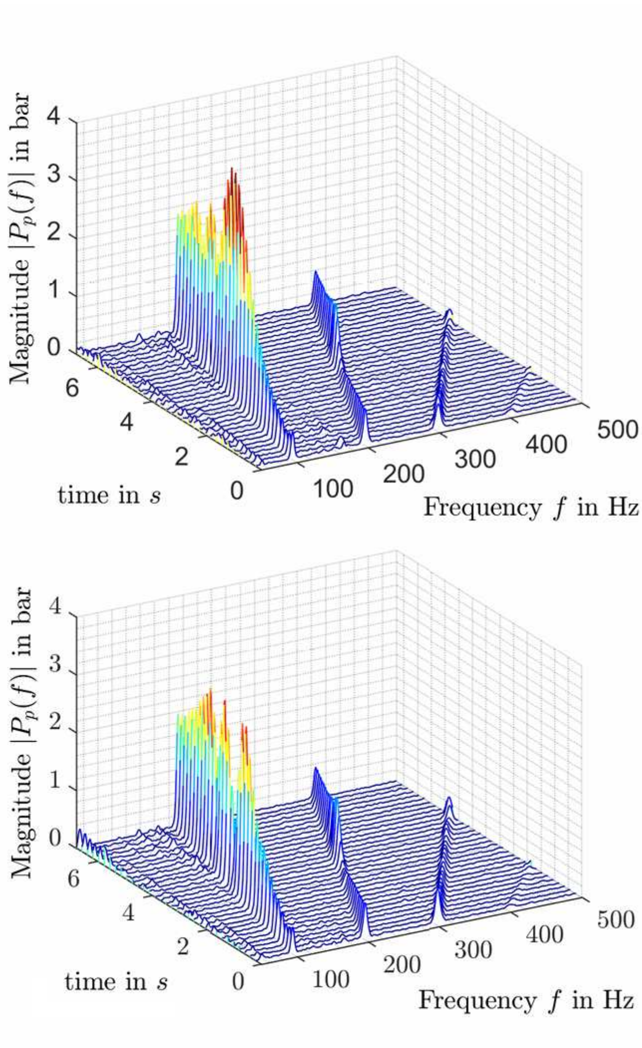


*Figure 10: STFT of the pressure at the pump outlet from the run-up measurement with closed pipeline, visualized as a 3D waterfall plot. Top: Without compensator, Bottom: With compensator*

amplitude over time was assumed, which does not account for the effect of rotor oscillations on dynamic pressure pulsations. Besides the narrowband characteristics, a difference appears when analysing secondary resonances. The simulations predict two secondary resonances, which leads to increased pulsations caused by the compensator. Neither in the time domain nor in the frequency domain measurements, secondary resonances appear that would degrade the system behaviour. The test setup was designed in such a way that the main resonance dominates the system behaviour. However, additional amplitude reductions are observed at 162 Hz in both measurements and at 173 Hz only in the reference measurement. Compared to the effect of the compensator coupling, these reductions are considered as negligible and are not further investigated.

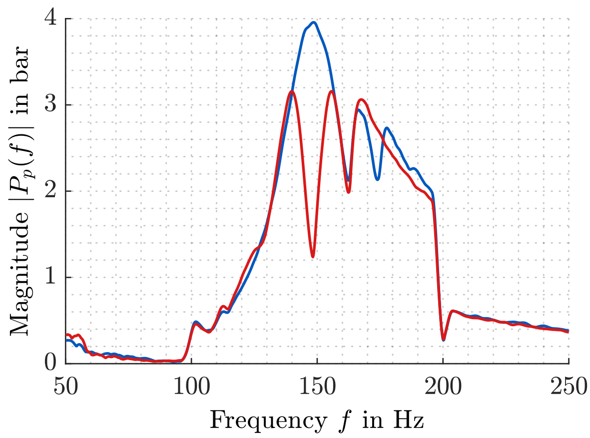


*Figure 11: Fourier transformed signal of the pressure at the pump outlet of the run-up measurement with closed pipeline, Blue: Without compensator, Red: With Compensator.*

## 5 Hydraulic system with cylinder

The second investigated scenario involves a cylinder chamber connected to the pump via a hose. The measurements primarily analyse the behaviour of the hydraulic system, with the cylinder in its limit stop position. For this configuration, the frequency response is first analysed through a simulation. Figure 12 illustrates the hydraulic system including all components relevant for the simulation. At the limit stop position, the piston chamber can be modelled as constant hydraulic capacity $C_C$ and the rod side can be neglected.

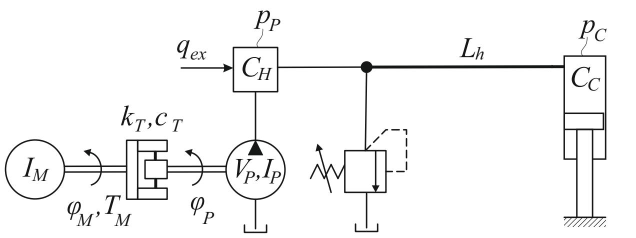


*Figure 12: Hydraulic system with cylinder in limit stop position.*

A dynamic laminar model is applied to describe the hose, considering the inlet and outlet pressure as the input ($p_P$ and $p_C$). For the calculation in the frequency domain, this can be written as

$$\begin{bmatrix} Q_H(i\omega) \\ Q_C(i\omega) \end{bmatrix} = \begin{bmatrix} S_{12} & T_{12} \\ T_{12} & S_{12} \end{bmatrix} \begin{bmatrix} P_P(i\omega) \\ P_C(i\omega) \end{bmatrix} \tag{8}$$

with

$$S_{12} = \frac{i \sin(2\gamma' L_h/i)}{Z'(\cos(2\gamma' L_h/i) - 1)}, \tag{9}$$

$$T_{12} = \frac{i}{Z'(\sin(\gamma' L_h/i) - 1)}, \tag{10}$$

$$Z' = \frac{\sqrt{E'\rho}}{r_P^2 \pi} \sqrt{-\frac{J_0(ir\sqrt{i\omega/\nu})}{J_2(ir\sqrt{i\omega/\nu})}} \tag{11}$$

and

$$\gamma' = \frac{i\omega}{\sqrt{E'/\rho}} \sqrt{-\frac{J_0(ir\sqrt{i\omega/\nu})}{J_2(ir\sqrt{i\omega/\nu})}}. \tag{12}$$

With the hose model and the cylinder represented as constant capacity, the system is described by equation (2), using the adapted system matrices **M**, **C** and **K**, according to the state vector **X** and the excitation vector **F**:

$$\mathbf{M} = \begin{bmatrix} I_M & 0 & 0 & 0 \\ 0 & I_P & 0 & 0 \\ 0 & -\frac{V_p}{2\pi} & C_H & 0 \\ 0 & 0 & 0 & C_C \end{bmatrix}, \quad \mathbf{C} = \begin{bmatrix} 0 & 0 & 0 & 0 \\ 0 & c_T & 0 & 0 \\ 0 & 0 & S_{12} & T_{12} \\ 0 & 0 & T_{12} & S_{12} \end{bmatrix},$$

$$\mathbf{K} = \begin{bmatrix} k_T & -k_T & 0 & 0 \\ -k_T & k_T & \frac{V_P}{2\pi} & 0 \\ 0 & 0 & 0 & 0 \\ 0 & 0 & 0 & 0 \end{bmatrix},$$

$$\mathbf{X} = \begin{bmatrix} \Phi_M(i\omega) \\ \Phi_P(i\omega) \\ P_P(i\omega) \\ P_C(i\omega) \end{bmatrix}, \quad \mathbf{F} = \begin{bmatrix} T_M(i\omega) \\ 0 \\ i\omega Q_{ex}(i\omega) \\ 0 \end{bmatrix}. \tag{13}$$

The simulation parameters for the system with the cylinder are listed in tab. 3 and tab. 4. The bulk modulus value for the hose is taken from [10].

*Table 4: Model parameters for the experiment with cylinder.*

| | | |
|---|---|---|
| $k_T$ | 2600 Nm/rad | Torsional stiffness |
| $E'$ | $0.6 \cdot 10^9$ Pa | Bulk modulus hose |
| $V_C$ | $1.8 \cdot 10^{-3}$ m$^3$ | Volume cylinder chamber |
| $L_h$ | 1.25 m | Hose length |
| $r_h$ | 8 mm | Hose inner radius |
| $C_C$ | $V_C/E$ | Capacity cylinder chamber |

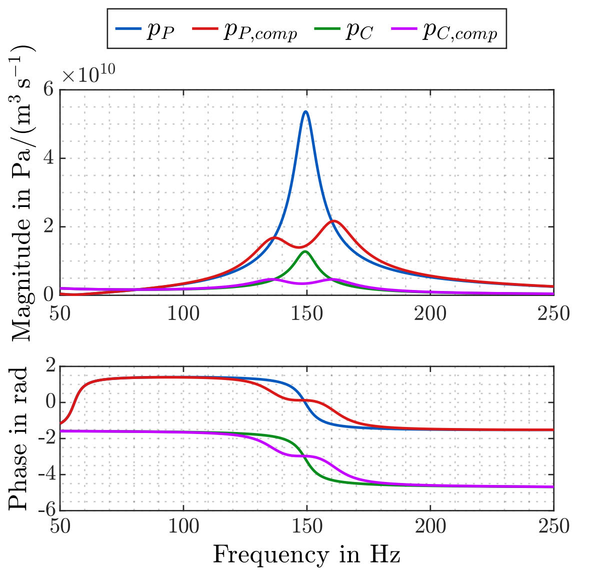


*Figure 13: Simulation results with cylinder as transfer functions between flow rate excitation and pressure. Blue & Red: Pressure at the pump outlet without ($p_P$) & with compensator ($p_{P,comp}$), Green & Purple: Pressure in the cylinder chamber without ($p_C$) & with compensator ($p_{C,comp}$).*

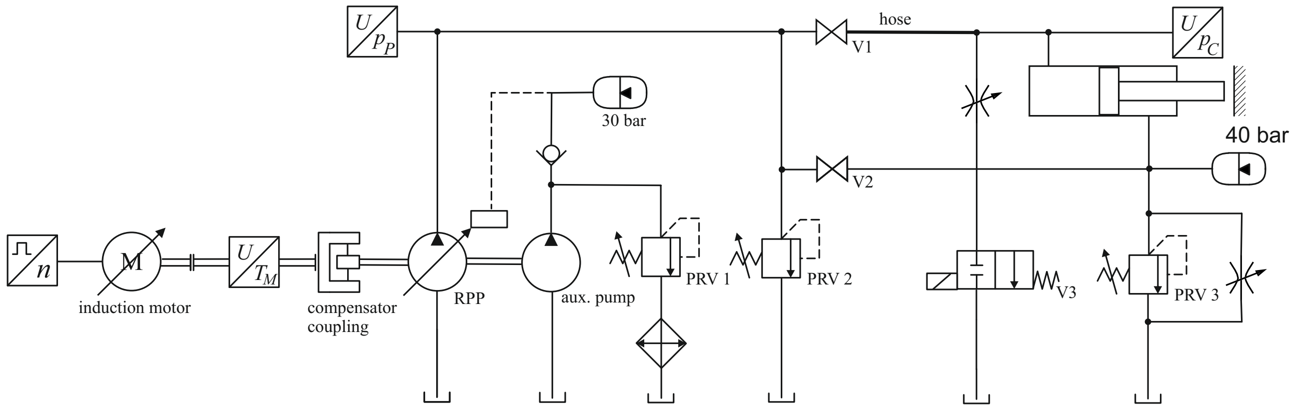


*Figure 14: Overall hydraulic layout including the drivetrain, with compensator coupling and a cylinder.*

Figure 13 shows the calculated transfer functions between flow rate excitation and pressure response at the pump outlet $G_{P_PQ}(i\omega) = P_P(i\omega)/Q_{ex}(i\omega)$ and in the cylinder chamber $G_{P_CQ}(i\omega) = P_C(i\omega)/Q_{ex}(i\omega)$. The length of the hose was adjusted so that the resonance frequency occurs near 150 Hz. By calculating the stiffness of the compensator coupling with equation (1), the compensation frequency was tuned for the simulation. The effect of the compensator is observed at both the pump outlet and the cylinder chamber.

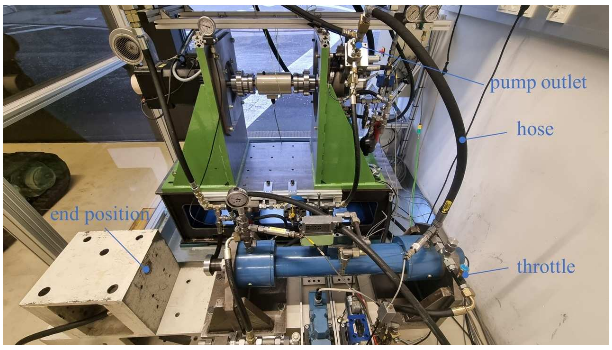


*Figure 15: Test rig with cylinder.*

Figure 14 illustrates a simplified layout of the hydraulic system used and fig. 15 shows the test rig including the cylinder. Based on the simulations results, the cylinder stroke limitation and the hose length were chosen. The dead volume of the cylinder and the bulk modulus of the hose were not exactly known. With all fittings, the hose length is approximately 1.3 m. To retract the cylinder after the experiment, a hydraulic accumulator is attached to the rod side of the cylinder. The line for filling the hydraulic accumulator is closed during the experiments by the shut-off valve V2. In order to prevent the closed filling line from influencing the system behaviour, the shut-off valve is directly installed on a second outlet of the pump block. The pressure relief valve PRV3 with closed parallel throttle limits the pressure in the hydraulic accumulator. During retraction, the switching valve V3 connects the piston side of the cylinder with the tank. To reduce the influence of the line to the switching valve, a throttle is installed near the cylinder chamber, which is almost closed for the experiments. During the experiments, the valve V1 is open and the valves V2 & V3 are closed. As in the previous experiments, the pressure is limited by the pressure relief valve (PRV 2 in fig. 14) at the pump outlet.

### 5.1 Run-up experiment with cylinder in limit stop position

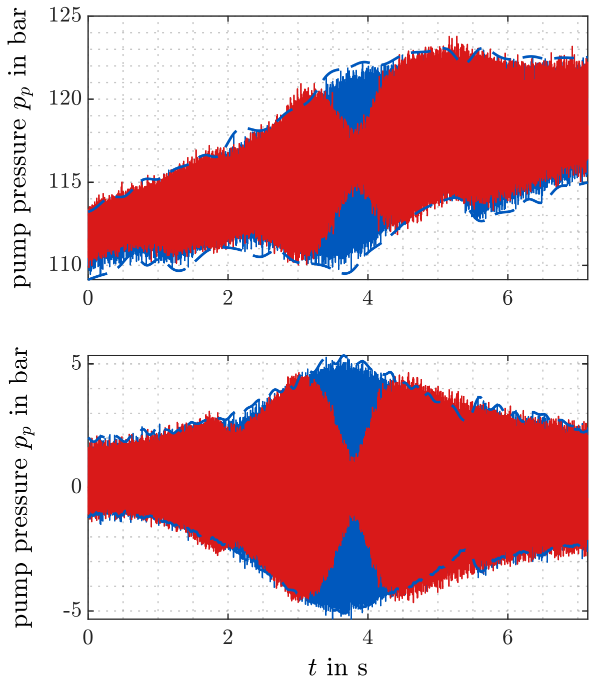


*Figure 16: Measurement results of the run-up experiment with cylinder in limit stop position. Blue: Without compensator, Red: With compensator. Top: Low-pass filtered signal of the pressure at the pump outlet, Bottom: Bandpass filtered signal of the pressure at the pump outlet.*

In this experiment, the cylinder is already at its limit stop position. The motor accelerates uniformly from 850 rpm to 1700 rpm while the pump generates a dominant excitation in a frequency range of 100 Hz to 200 Hz. Figure 16 shows the measurement result in the time domain. The upper illus-

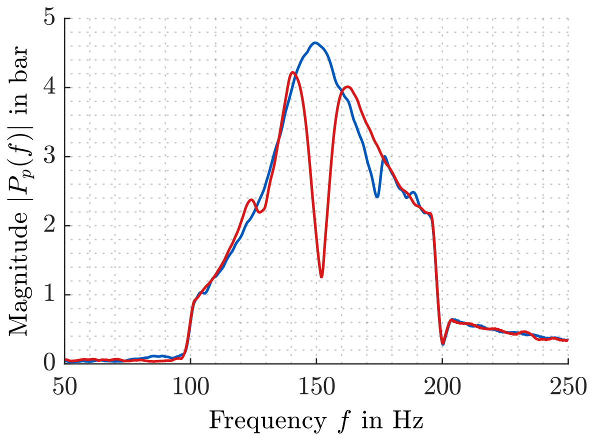


*Figure 17: Fourier transformed signal of the pressure at the pump outlet, run-up measurement with cylinder in limit stop position. Blue: Without compensator, Red: With Compensator.*

tration displays the low-pass filtered signal (cut-off frequency 1000 Hz) with and without compensator. After approximately 3.7 seconds, the largest notch in the pressure signal occurs. At the bottom of fig. 16 the bandpass filtered signal is shown. The bandpass filter has a passband frequency from 50 Hz to 250 Hz. The measurement without the compensator shows a pressure pulsation amplitude of 4.7 bar, whereas with the compensator, it is 1.1 bar. Figure 17 displays the pressure signal in the frequency domain. As in the experiment with the closed pipeline, significant compensation occurs at approximately 150 Hz. In contrast, secondary resonances are clearly noticeable. The increased pressure pulsation at the secondary resonances can be observed in the bandpass filtered pressure signal in the time domain. After 4.3 seconds the amplitude of the reference measurement is slightly lower than the amplitude of the measurement with the compensator. Significant improvements in system behaviour occur in the frequency range from 142 Hz to 158 Hz.

Figure 18 illustrates the pressure in the cylinder chamber in the time domain. On top the low-passed filtered signals (cut-off frequency 1000 Hz) are shown. No constriction of the amplitude is visible. Through further signal processing in the form of a bandpass filter with a passband frequency from 50 to 250 Hz, the compensator effect becomes apparent, which is shown at the bottom. The Fourier transformed signal in fig. 19 reveals that the second harmonic frequency, at approximately 350 Hz, oscillates significantly higher than the first. In all previous measurements, the amplitudes at the second harmonic frequency were significantly lower than the amplitudes at the first and were therefore not taken into account. The highest pulsation is observed after 5.4 seconds in fig. 18. At this point, the motor drives the pump at 1500 rpm. Equation (7) gives an excitation frequency of 175 Hz. This is consistent with the observations from the frequency analysis.

### 5.2 Extending experiment to limit stop position

In the previous investigations, the experimental setup used the combination of a speed controlled motor and a pump with constant displacement volume. In another experiment, the motor operates at a constant speed of 1280 rpm, resulting in a dominant excitation frequency of approximately 148 Hz. At the beginning of the experiment, the displacement of the pump is set to 0 $cm^3/rev$ and the cylinder is fully retracted. To extend the cylinder to its limit stop position, the displacement of the pump is set to its maximum of 32 $cm^3/rev$. Figure

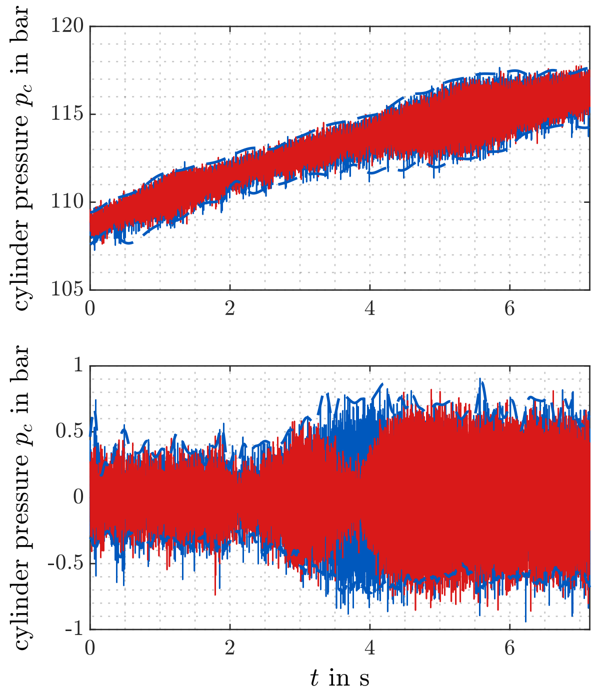


*Figure 18: Measurement results of the run-up experiment with cylinder in limit stop position. Blue: Without compensator, Red: With compensator. Top: Low-pass filtered signal of the pressure in the cylinder chamber, Bottom: Bandpass filtered signal of the pressure in the cylinder chamber.*

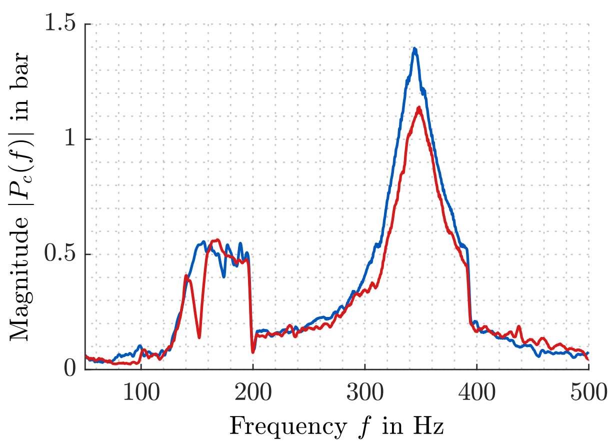


*Figure 19: Fast Fourier transformed signal of the pressure in the cylinder chamber, run-up measurement with cylinder in limit stop position. Blue: Without compensator, Red: With compensator.*

20 shows the pressure signal at the pump outlet. During the first 2.8 seconds the cylinder extends and the pressure in the piston chamber increases due to the hydraulic accumulator on the rod side. At the beginning, the compensator has no significant effect on the pressure pulsation. Due to the undesirable dependency between drivetrain torque and compensation frequency, the compensator is misadjusted in that case. As the pressure increases, the system gets closer to the operating range of the compensator. Just before reaching the limit stop position at 2.8 seconds, a reduction in pressure pulsation becomes noticeable. At the end position, where the compensator is well tuned, the pressure amplitude decreases by a factor of two. The measurement confirms that the compensator coupling achieves significant improvements at the correct operating point.

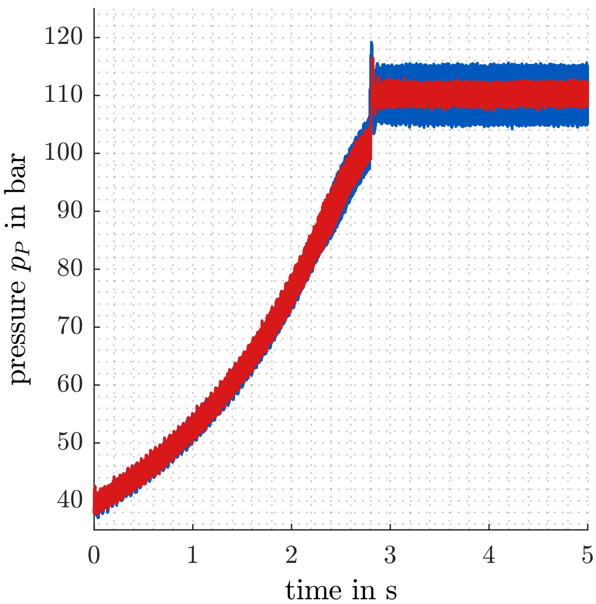


*Figure 20: Measurement result from extending cylinder to limit position. Blue: Pressure signal at the pump outlet without compensator, Red: Pressure signal at the pump outlet with compensator, both low-pass filtered at 1000 Hz.*

## 6 Conclusion and outlook

Investigations with different hydraulic systems in hydraulic resonance were made using the compensator coupling in the drivetrain. The measurement results demonstrate that significant improvements can be achieved with this type of compensator at the compensation frequency. In the case of hydraulic resonance, the amplitude of the pressure pulsation was reduced by a factor greater than three. The experiments also showed that the compensator coupling, in combination with the radial piston pump, is narrowband and exhibits an undesirable dependence between torque and compensation frequency. The dependence is particularly unfavorable for a narrowband compensator, whereas it may be negligible for a broadband one. To increase the bandwidth of the compensator, lower inertia on the pump side is required.

Therefore, investigations with gear pumps, which exhibit a significantly lower inertia than the used radial piston pump, are planned as a next step. For the next prototypes, new designs are being investigated, whose torsional stiffness should be independent of the operating conditions. Once a broadband rotary mechanical pulsation compensator has been developed, comparative measurements can be carried out with other compensation systems, such as the Helmholtz resonator, to allow a direct comparison of their performance under identical conditions.

## References


[1] M Stosiak, I Yatskiv, O Prentkovskis, and M Karpenko. Reduction of Pressure Pulsations over a Wide Frequency Range in Hydrostatic Systems. Machines 13(1), 25, 2025. DOI: 10.3390/machines13010025.

[2] Y Wang, T Shen, C Tan, et al. Research Status, Critical Technologies, and Development Trends of Hydraulic Pressure Pulsation Attenuator. Chin. J. Mech. Eng. 34, 14, 2021. DOI: 10.1186/s10033-021-00532-z.

[3] J Mikota and H Reiter. Development of a compact and tuneable vibration compensator for hydraulic systems. *International Journal of Fluid Power*, 4(1):17–31, 2003. DOI: 10.1080/14399776.2003.10781152.

[4] G Mikota. Vorrichtung zur Reduktion von Druckpulsationen in einem Hydrauliksystem. Austrian Patent AT 526449 B1, 2024.

[5] G Mikota and B Manhartgruber. A novel pulsation compensator for displacement machines. In *Proceedings of 14th International Fluid Power Conference*, pages 395–406, Dresden, Germany, March 19-21, 2024. DOI: 10.13052/rp-9788770042222C30.

[6] G Mikota. Design and Simulation of a Drivetrain Integrated Pulsation Compensator for Pumps. In *BATH/ASME 2024 Symposium on Fluid Power and Motion Control*, Bath, England, September 11-13, 2024. V001T01A008. DOI: 10.1115/FPMC2024-140002.

[7] J Rametsteiner. Entwicklung einer torsionselastischen Tilgerkupplung für eine Radialkolbenpumpe. Bachelor's thesis, Johannes Kepler University, Institute of Machine Design and Fluid Power, Linz, August, 2024.

[8] A F D'Souza and R Oldenburger. Dynamic Response of Fluid Lines. *Transactions of the ASME - Journal of Basic Engineering*, 86:589–598, 1964. DOI: 10.1115/1.3653180.

[9] J Ivantysyn and M Ivantysynova. *Hydrostatische Pumpen und Motoren*. Vogel Verlag und Druck KG, Würzburg, Germany, 1993.

[10] D Will and N Gebhardt. *Hydraulik Grundlagen, Komponenten, Schaltungen*. Springer, 2011. 5. Auflage, S. 21, DOI: 10.1007/978-3-642-17243-4.